Proceedings of Global Power and Propulsion Society
ISSN-Nr: 2504-4400
GPPS Hong Kong 2023
October 17-19, 2023
www.gpps.global

# GPPS-TC-2023-0078

# RESEARCH ON MATCHING FAILURE MECHANISM OF LOW-PRESSURE TURBINE UNDER LOW WORKING CONDITION

**Han Zhang**
**College of Power and Energy Engineering,**
**Harbin Engineering University**
Email1811668089@qq.com
Harbin, Heilongjiang, P.R.C

**Lei Wu**
**College of Power and Energy Engineering,**
**Harbin Engineering University**
s321wulei@hrbeu.edu.cn
Harbin, Heilongjiang, P.R.C

**Xuan Zuo**
**College of Power and Energy Engineering,**
**Harbin Engineering University**
2774057305@qq.com
Harbin, Heilongjiang, P.R.C

**Jie Gao***
**College of Power and Energy Engineering,**
**Harbin Engineering University**
gaojie_d@hrbeu.edu.cn
Harbin, Heilongjiang, P.R.C

**Dongchen Huo**
**College of Power and Energy Engineering,**
**Harbin Engineering University**
Huodchen@hrbeu.edu.cn
Harbin, Heilongjiang, P.R.C

## ABSTRACT

In order to clarify the failure mechanism of low-pressure turbine matching under low working conditions, the numerical simulation of a low-pressure turbine under design condition and low working conditions are carried out. The results show that under low working conditions, the isentropic expansion efficiency of the low-pressure turbine decreases by more than 1.69%. Large total pressure losses exist on both vane and rotor in low pressure turbine. The upper passage vortex core moves down and the lower passage vortex core moves up, and low energy fluid in the endwall boundary layer flows to the midspan. Under the influence of low energy fluid from the vane trailing edge, the size and intensity of the tip leakage vortex in 95% vane span becomes larger, and the large passage vortex appears at the midspan of the rotor. The reduced turbine efficiency is mainly caused by low energy fluid from vane trailing edge, tip leakage vortex of the rotor and passage vortex of the midspan of the rotor.

**Keywords:** Low pressure turbine, Low working condition, Aerodynamic performance, Match deterioration

## INTRODUCTION

With the global energy crisis and the rapid development of science and technology, the requirements for energy efficiency of existing power device are becoming more and more stringent [1]. The low-pressure turbine has many stages and blades, which is one of the important components affecting the efficiency and quality of gas turbines. The fuel gas expands in the turbine passage to provide work capacity. The main losses in turbine passage include blade profile loss, secondary flow loss at the blade endwall and leakage loss caused by rotor tip clearance [2]. The meridional plane of the low-pressure turbine and power turbine of the marine gas turbine usually takes the form of large meridional expansion, which will cause more intense secondary flow at the endwall, thus causing strong flow loss in the endwall field [3]. Sieverding [4] and Langston [5] gave a detailed review of the secondary flow phenomenon and the vortex model in cascades, mainly describing the formation of horseshoe vortex on the leading edge in the secondary flow, the vortex structure in the cascade passage and the interaction between the vortices in the passage. Through aerodynamic experiments on turbine cascades, Zhang [6] et al. found that the loss in the endwall field was caused by the secondary flow interaction between the blade surface and the endwall boundary layer and the secondary kinetic energy dissipation of the vortex.

Mayle [7] found that when the low-pressure turbine works at low Reynolds number, its suction surface may be separated, causing serious aerodynamic losses and reducing the efficiency of the turbine. Hourmouziadis [8] pointed out that the lower the Reynolds number, the easier the boundary layer separation occurs, which changes the flow state of the

boundary layer on the suction surface and further affects the blade profile losses and secondary flow losses. Domestic researches on the internal flow mechanism of low-pressure turbine had also achieved fruitful results. Ye [9] used the large eddy simulation method to study the temporal and spatial evolution mechanism of cascade boundary layer under low Reynolds number conditions, and investigated the separation transition process of laminar boundary layer under low Reynolds number conditions. Qiao et al. [10] found that the smaller the Reynolds number, the closer the separation point of the boundary layer of the suction surface was to the leading edge, and the total pressure loss behind the cascade, the width of the wake zone and the velocity loss all increased through cascade experiments. Yue et al. [11] found that with the decrease of Reynolds number, the total pressure loss of cascade outlet section gradually increased, and the average loss value and the increase range of high loss area showed a nonlinear growth trend.

Meng [12] carried out that the change of inflow turbulence had little effect on the overall total pressure loss of the blade passage, but obvious effect on the composition of the loss. The increase of inflow turbulence intensity significantly increased the blade profile loss and reduced the loss caused by the wall boundary layer at the same time. Increasing the turbulence intensity would generate an increase in the turbulence intensity of the boundary layer, which was conducive to resist boundary layer separation in the mid-rear of the blade.

Curits et al. [13] found that the aerodynamic loss was caused by the suction surface accounted for 60% blade profile loss. Cao et al. [14] studied the effect of wake on the flow characteristics and transition process of the boundary layer on the suction surface of the low-pressure turbine blade. It was found that during the trail intermission, the trail-induced turbulence field and the suppression field still affected the development of the boundary layer on the trailing edge of the blade, and the separation bubble was regenerated upstream of the suppression field. Teng [15] found that the boundary layer of the suction surface undergone reattachment separation under steady regime, and the periodic wake inhibited the separation of the boundary layer of the suction surface through experiments.

Most domestic and international scholar have studied the influence of single variables, such as Reynolds number, inflow turbulence and upstream trail, on the internal flow field of low-pressure turbine through experimental and numerical methods. However, there are few studies on the complex flow field inside the low-pressure turbine cascade and the matching failure mechanism between low condition stages under partial load conditions. Therefore, it is necessary to conduct in-depth research on the failure mechanism of low-pressure turbine inter-stage matching under low working conditions.

## NUMERICAL METHOD

### The numerical simulation

In this paper, the computational fluid software ANSYS CFX 18.0 was used for numerical calculation of the turbine to solve the three-dimensional fixed length Reynolds average equations Navier-Stokes equations. The Shear Stress Transport (SST) model combines the advantages of the $k-\omega$ model and the $k-\varepsilon$ model. The $k-\omega$ model is used to capture the viscous sublayer flow near the wall, while the $k-\varepsilon$ model is used to predict the flow in the mainstream region, which is more accurate and reliable for the simulation of practical problems. Therefore, the SST turbulence model is selected in this paper.

AutoGrid5 in NUMECA is used to conduct structured grid division for turbine vane and rotor blade. O-mesh grid is used in the near wall area of the cascade, and H-mesh grid is used in the far wall area. At the same time, the leading edge and trailing edge of the blade are encrypted. The grid distance of the first layer near the wall of the model is set to 0.001 mm to meet the requirements of the SST turbulence model for $y^+$.

### Computational grids

In order to make the calculation results more accurate, seven kind of grid numbers are divided for grid sensitivity verification.

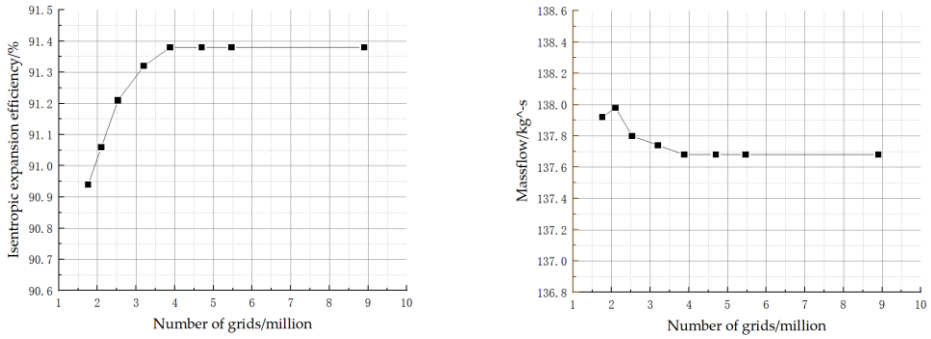


(a) Variation of efficiency with the number of grids (b) Variation of massflow with the number of grids

**Figure 1 Low pressure turbine mesh sensitivity verification**

Figure 1 shows the effects of different grid numbers of 1.76 million, 2.1 million, 2.53 million, 3.2 million, 3.88 million, 4.7 million, 5.47 million and 8.9 million on the efficiency and flow rate of low-pressure turbine. Figure 1 shows that when the number of grids is over 3.88 million, the efficiency and flow rate basically do not change with the change of grid number. Therefore, the number of model grids is 3.88 million.

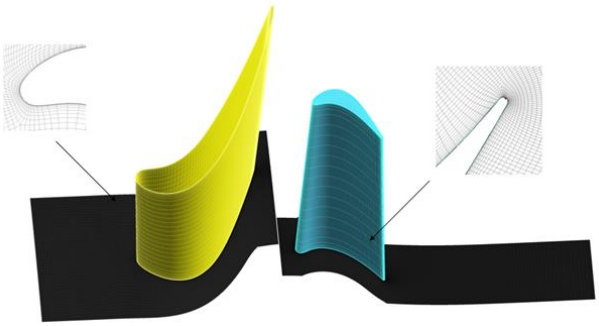

**Figure 2 Mesh of rotor blade and vane**

Figure 2 is a schematic diagram of the meshing of the rotor and vane of the low-pressure turbine model.

### Low working conditions boundary

In order to find out the main reason for the loss function of efficiency in low pressure turbine under partial load conditions, the internal flow field of condition 1 and condition 2 shown in Table 1 are selected for analysis. Among them, ' 70 % ' represents 70 % design speed of low-pressure turbine. The pressure ratio in condition 1 is 90% of the designed pressure ratio, and the pressure ratio in condition 2 is 70% of the designed pressure ratio.

**Table 1 Turbine performance at two partly loaded conditions**

| Condition | Relative rotation speed | Relative expansion ratio/% |
|---|---|---|
| Condition 1 | 70% | 90 |
| Condition 2 | 50% | 70 |

## RESULTS AND DISCUSSION

### Flow field state of vane under low working conditions

Under low working conditions, the change of the inlet boundary conditions will significantly change the aerodynamic parameters and losses in the low-pressure turbine. Figure 3 shows the distribution curve of the total pressure loss coefficient at vane outlet along the vane span for the design condition, condition 1 and condition 2. The total pressure loss coefficient at vane outlet is:

$$Y_1 = \frac{P_0^* - P_1^*}{P_1^* - P_1} \tag{1}$$

In formula (1), $P_0^*$、$P_1^*$ is the inlet and outlet total pressure of vane;$P_1$ is the static pressure of vane outlet.

For the convenience of describing each definition, DC indicates the design condition, while C1 is condition 1 and C2 is condition 2.

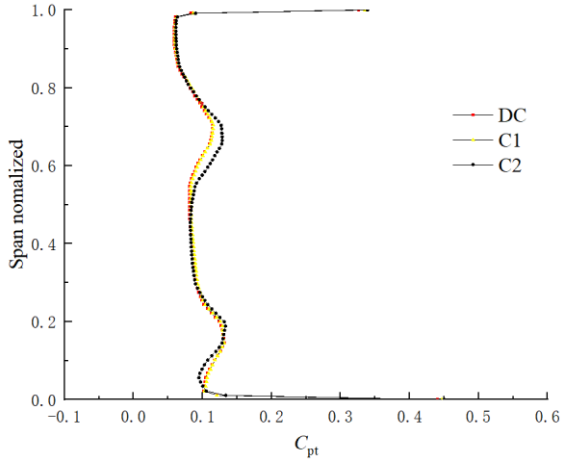


**Figure 3 Total pressure loss coefficient at the outlet of each condition of the vane**

In Fig. 3, the total pressure loss coefficient under C1 is basically the same as that under DC, and the vortex scale of the upper and lower passages of two conditions is same. At 50 % ~75 % vane span, the total pressure loss coefficient of vane is relatively large. Compared with DC, the total pressure loss coefficient under C2 increases by 0.02~0.03, and the vortex inch of the upper passage is larger, but the vortex core moves to midspan. At 13% ~20% vane span, the total pressure loss coefficient of C2 increases by 0.005 ~ 0.015 compared with DC, but the vortex scale of the lower passage becomes smaller and the vortex core moves to midspan. At 3 % ~ 13 % vane span, the total pressure loss coefficient under C2 is 0.01 ~ 0.02 lower than that under DC.

In Fig. 3, the flow loss most changes at 50% to 75% vane span, 13% to 20% vane span, and 3% to 13% vane span under low working conditions. Therefore, in order to carry out the flow behaviours at these three flow fields, Fig. 4 shows the distribution curves of the static pressure coefficient of the blade surface at 5%, 18% and 68% vane span of the low-pressure turbine under different working conditions. The static pressure coefficient $C_p$ is the ratio of local static pressure to the total pressure at mainstream inlet.

In Fig.4, it is found that the load of vane suction surface changes greatly under low working conditions, while the load of pressure surface does not change under three working conditions. At 5% vane span and about 60% axial chord, the capacity for work under C2 is stronger than that under DC and C1. After about 65% of the axial chord of the suction surface, there are obvious reverse pressure gradients under three working conditions. The reverse pressure section under DC and C1 consists of two small reverse pressure sections and a reverse pressure section with a large reverse pressure gradient, while the reverse pressure section of the C2 has a smaller reverse pressure gradient.

At 18% vane span, the blade load under the three working conditions is similar to that at 5% vane span, but the work capacity under C2 before 65% axial chord position is weaker than that under DC and C1. At the field of 68% vane span and about 70% axial chord, there are inverse pressure gradients in all three working conditions, among which, inverse pressure gradient: C2 < C1 < DC.

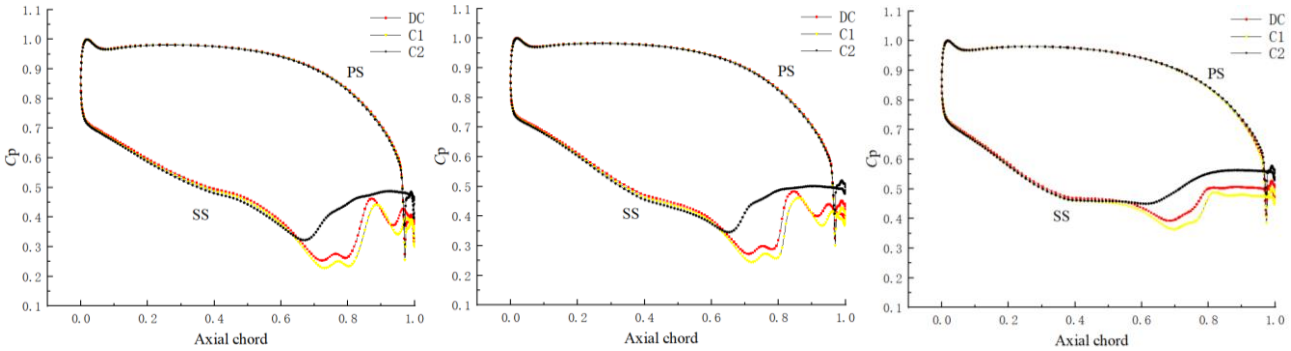


(a) 5% vane span (b) 18% vane span (c) 68% vane span

**Figure 4 Static pressure coefficient at 5%、18% and 68% of vane span of low-pressure turbine**

In order to intuitively study the vortex structure of the vane of the low-pressure turbine under three working conditions, Fig. 5 shows the vortex structure diagram from the downstream to the upstream view. The following vortex core display method is adopted: Q-criterion.

The physical explanation of vortex core is that vorticity is larger than strain ratio, namely:

$$Q = -\frac{1}{2}u_{i,j}u_{i,j} = \frac{1}{2}(\|\omega\|^2 - \|S\|^2) \tag{2}$$

Where $\omega$ and $S$ are rotation and strain tensors. The relative total pressure loss coefficient is used to color the vortex structure to show the magnitude of its local loss.

From figure 5, it can be clearly identified that the main vortex structures in the passage are passage vortex and shedding vortex. In Fig.5, PV is the passage vortex, SV is the shedding vortex, SP is the stagnation point, SHV is the suction surface horseshoe vortex, PHV is the pressure surface horseshoe vortex. Because the meridional expansion angle of the upper endwall is larger than that of the lower endwall, the field of the upper passage vortex is farther away from the upper endwall, and the separation of the upper passage vortex is more serious. The passage vortex and the shedding vortex are coupled in the front of the vane suction, flowing to the downstream blade row and separating from each other. It can be seen from Fig.5 that, compared with the DC, the upper passage vortex and the upper shedding vortex change little, while the lower passage vortex becomes larger and the lower shedding vortex becomes smaller under low working conditions. Especially in C2, the separation point of the lower passage vortex and the lower shedding vortex moves forward to the leading edge, while the DC is the opposite.

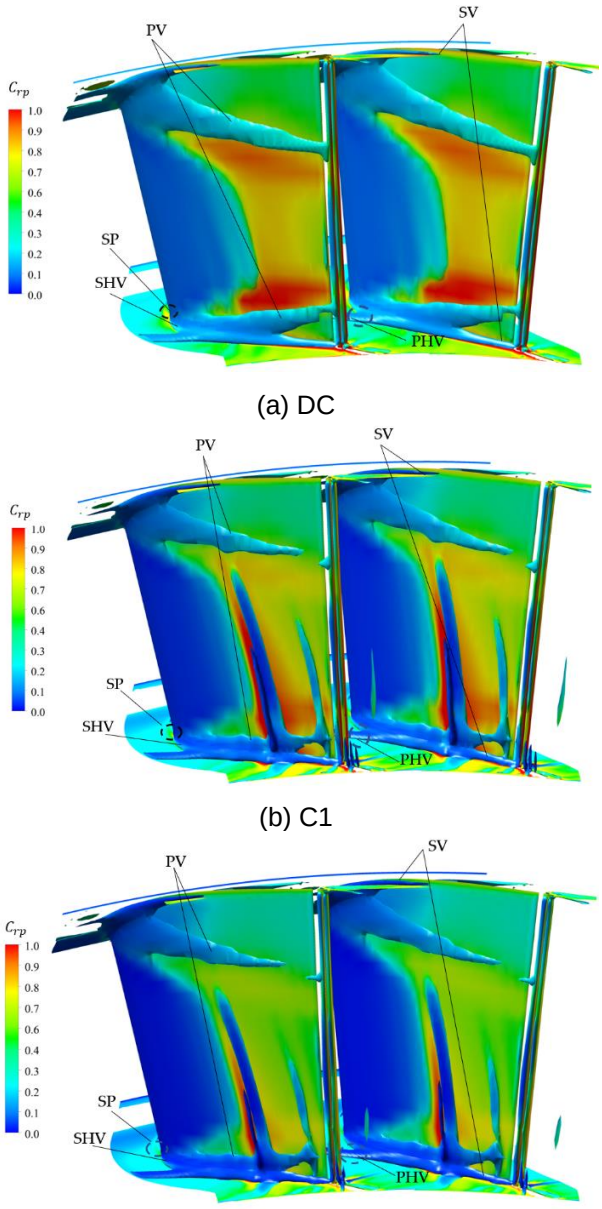


(a) DC

(b) C1

(c) C2

**Figure 5 Vortex structures of vane by isosurface of Q-criterion**

### Flow field state of rotor under low working conditions

Fig.6 shows the distribution curve of the total pressure loss coefficient at rotor outlet along the relative blade span under different working conditions. On the whole, due to the influence of the upstream low-energy fluid, the total pressure loss coefficient of the rotor outlet under low working conditions is 1 to 2 times that of the total pressure loss coefficient under DC. In C1, under the influence of the lower passage vortex in the flow field of the upstream vane, the total pressure loss coefficient obviously peaks at 30 % blade span. Due to the interaction between the upper passage vortex in the upstream vane passage and the leakage vortex caused by the tip clearance of the rotor, the total pressure loss coefficient at 90 % of the rotor span is significantly larger than that of other fields. At about 30% relative blade span is the field of the lower passage vortex. The distribution of total pressure loss along the blade span under C2 is similar to that of C1, but the lower passage vortex in the upstream vane passage is larger under C2, so the peak size is larger at about 47 % of the relative blade span, which indicates that the passage vortex scale is larger here.

Figure 7 shows the distribution curve of the static pressure coefficient of the rotor blade along the dimensionless axial chord under low working conditions. By observing the change of blade surface load under different working conditions, it is found that under low working conditions, there is a low-pressure field in front of the 20 % axis chord in front of the blade suction surface due to the influence of the low energy fluid flowing out of the upstream vane flow field. At 50% and 95% of the blade span, due to the interaction between the upflow low energy fluid and the tip leakage vortex of the rotor, C1

and C2 are changed from uniform loading to forward loading, and the flow fields are more complicated.

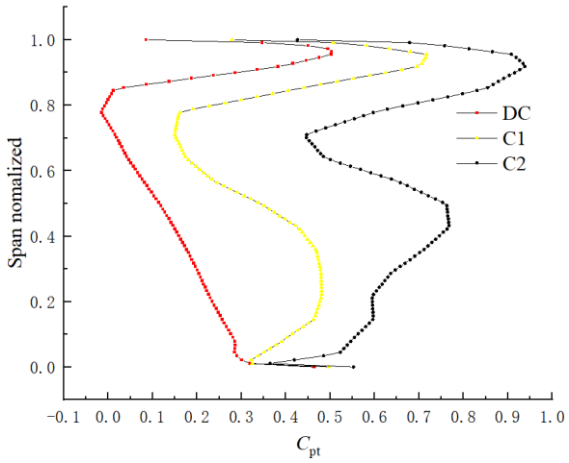


**Figure 6. Total pressure loss coefficient at the outlet of each condition of the rotor**

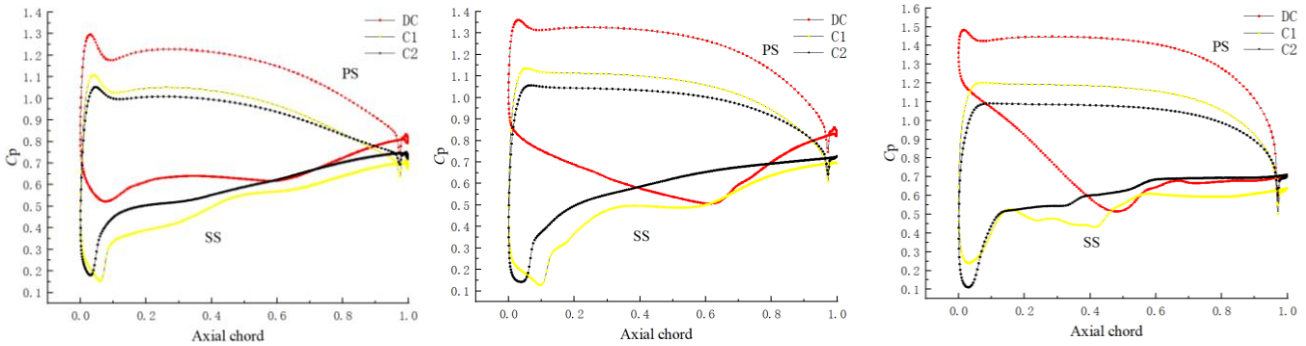


(a) 5% rotor span (b) 50% rotor span (c) 95% rotor span

**Figure 7 Static pressure coefficient at 5%、50% and 95% of blade span of low-pressure turbine**

According to the three-dimensional flow fields structure of the rotor blade cascade in Fig. 8, under low working conditions, due to the flow into the flow field of the rotor flow more disorder, the leakage vortex and corner vortex on the suction side increase significantly, and the flow on the suction side is more disordered. In C2, the range of leakage vortex accounts for about 30% of the blade span. It can be seen from the distribution of entropy increase cloud diagrams at different sections of the blade. The entropy increase of C2 is the largest.

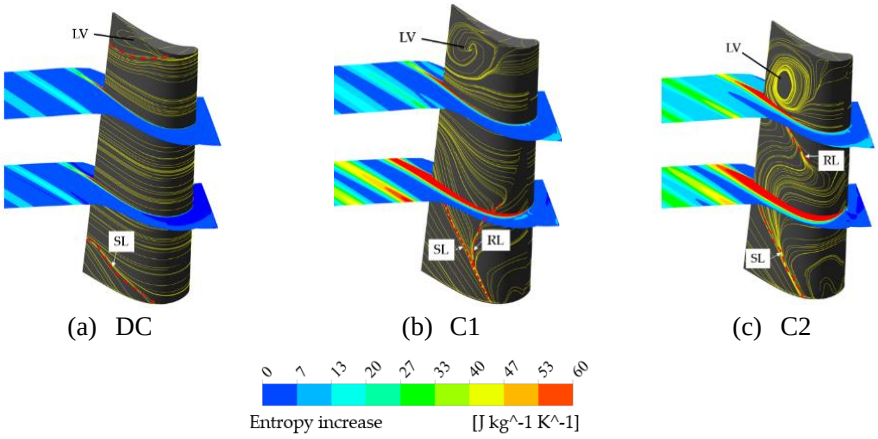


(a) DC (b) C1 (c) C2

**Figure 8 Flow field structures on rotor blade surface of low-pressure turbine at different conditions**

In Fig.8, LV is leakage vortex, SL is separation line, RL is reattached line.

Figure 9 is the entropy increase cloud diagram of each section in the passage under different working conditions. Combined with the correlation analysis results of Fig.7 ~ 9, it can be seen from the comparison of the entropy increase cloud diagrams of each section of the passage under each working condition in the figure that at C1, the overall loss of the suction surface and the scale of the tip leakage vortex become larger due to the influence of the low-energy fluid generated by the shedding vortex and the broken vortex at the trailing edge of the upstream vane. A large range of channel vortex appears at about 40% of the blade height, and a strong wake loss occurs at the outlet of the suction surface. In C2, the scale of the leakage vortex at the blade tip and the size of the passage vortex are bigger. The vortex core moves to the blade tip, and the wake loss at the outlet of the suction surface is bigger.

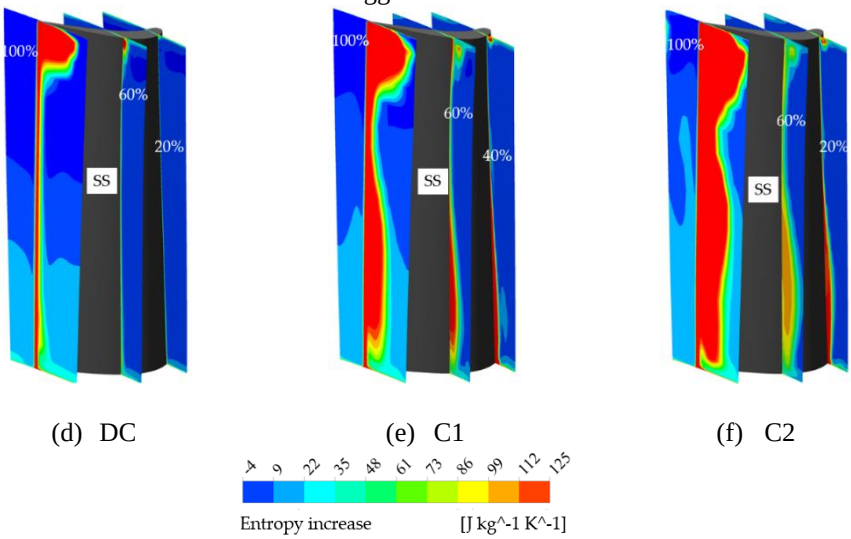


(d) DC (e) C1 (f) C2

**Figure 9 Entropy increase cloud diagram of each section in the passage of rotor at different conditions**

### Overall flow field analysis of low-pressure turbine stage under low working conditions

In order to make clear the causes of matching failure in low pressure turbine under low working conditions, the density gradient cloud diagram under different working conditions is analysed, as shown in Fig.10.

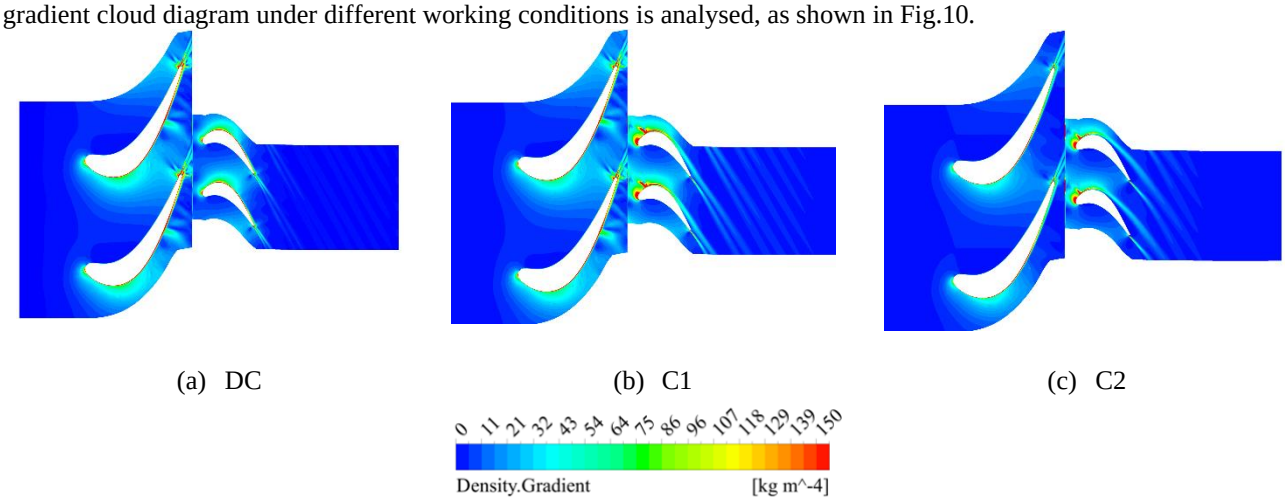


(a) DC (b) C1 (c) C2

**Figure 10 Low pressure turbine density gradient cloud diagram under different working conditions**

It can be seen in Fig.10 that compared under DC, the flow field distributions under C1 and C2 are similar, and A small range of high-speed areas appeared at the suction front edge of the blade. The flow field begins to separate at 50% of the axial chord of the suction surface due to the underdeflection of the incoming flow in the rotor flow field caused by the inflow of low energy fluid from the upper stream.

The change of the vane inlet boundary condition will change the inlet flow angle of itself and the downstream blade, which will affect the flow behaviours in the downstream blade passage. In order to research the change of the relevant flow angle under low working conditions, Fig.11 shows the distribution curves of the flow angle of the vane outlet and the rotor inlet along the blade span under low working conditions.

According to Fig.11 (a), when the blade span is below 30%, the vane outlet flow angle under DC and C1 almost overlap. However, when the blade span is above 30%, the outlet flow angle under C1 is larger than that under DC. When the blade span is below about 45%, the outlet flow angle under C2 is smaller than that under DC, which will result in the

over-deflection of the airflow. When the blade span is about 45% ~ 70%, the outlet flow angle of the vane in C2 is larger than that in DC and C1, which indicates that the flow here is under-deflection under low working condition.

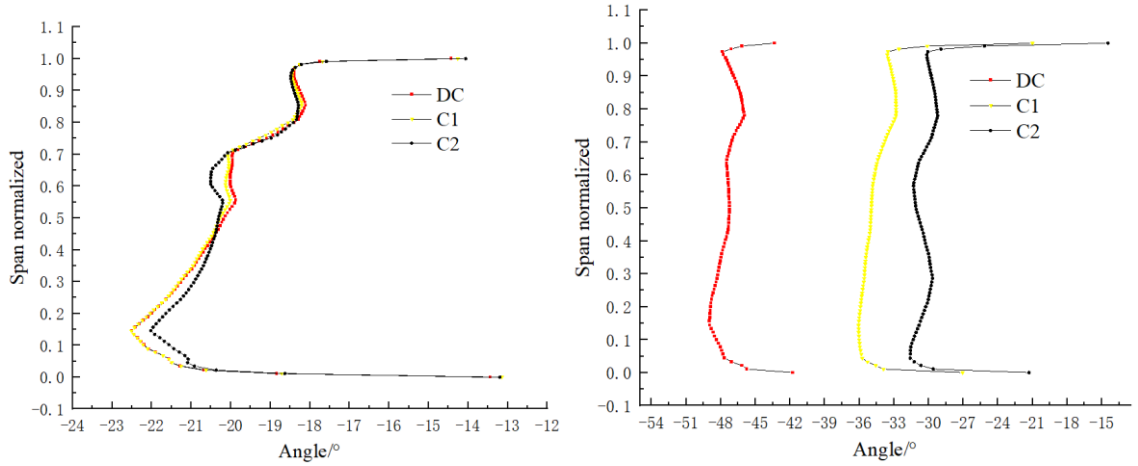


(a) Airflow angle distribution curves of vane outlet (b) Airflow angle distribution curves of rotor inlet

**Figure 11 Airflow angle distribution curves of vane outlet and rotor inlet along blade span under three conditions**

The change of the vane outlet flow angle will inevitably affect the downstream rotor inlet flow angle. It can be seen in Fig.11 (b) that under low working conditions, due to the flow from the upstream into the fluid more disorder, the rotor inlet flow angle decreases rapidly, which results in the deflection of the airflow. In C2, there is a peak at about 30 % blade span which is slightly smaller than other blade spans, which will indicate that the size of the passage vortex becomes larger under low working conditions.

On the whole, under low working conditions, the stagnation point of the horseshoe vortex at the leading edge of the rotor moves to the pressure surface, and the horseshoe vortex on the pressure surface becomes smaller, A large range of low speed and high loss areas appear at the rear of the suction surface.

## CONCLUSIONS

In order to explore the matching failure mechanism of low-pressure turbine stages under low working conditions, this paper researches the aerodynamic performance of low-pressure turbine stages under DC, C1 and C2 by numerical simulation method, and draws the following:

(1) In the vane fluid passage, the flow field distribution and load of C1 are similar to the DC, but in the second half of the suction surface, the transverse pressure difference of the vane of C1 is larger, which indicates that there is a large load here.

(2) Compared with the DC, in C2, the scale and strength of the upper and lower passage vortex in the vane flow field passage and the total pressure loss become larger. The scale of the lower shedding vortex becomes smaller. And the separation point of the lower passage vortex and the lower shedding vortex moves forward. The suction surface has a long reverse pressure gradient section from the 60% axial chord to the outlet, and the boundary layer of the suction surface grows faster in this section.

(3) In the rotor fluid passage, the total pressure loss in the flow field is mainly concentrated in the blade tip field. In C1 and C2, due to the influence of the upstream low-energy fluid, the gas flowing into the rotor passage is more disordered, so that the airflow is insufficiently deflected in the rotor passage, resulting in a significantly larger tip leakage vortex, and a larger and stronger passage vortex appears at the blade. The high loss field on the suction side moves to the leading edge, and the strong trail loss appears at the outlet of the suction surface. At 50 % and 95 % rotor span, load distributions of C1 and C2 change from uniform loading to front loading, which is not conducive to the improvement of flow state.

(4) Under low working conditions, the aerodynamic loss of the large meridional expansion low-pressure turbine mainly sources from the front of the rotor suction, the trail field and the junction of the suction surface separation field and the mainstream field. The stagnation point of the horseshoe vortex at the leading edge of the rotor moves to the pressure surface, and the horseshoe vortex on the pressure surface becomes smaller, there is a large range of low speed and high loss area at the rear of the suction surface. Therefore, the fine control of the incoming flow in the upstream vane flow field and the modification and optimization of the leading edge of the rotor may weaken the flow separation at the trailing edge of the rotor, thereby improving the turbine efficiency under low working conditions. This provides a certain reference for the subsequent fine control of inter-stage matching.

## NOMENCLATURE

| | |
|---|---|
| $P_0^*$ | inlet total pressure, MPa |
| $P_1^*$ | outlet total pressure, MPa |
| $P_1$ | static pressure of vane outlet, MPa |
| $C_p$ | static pressure coefficient |
| $\omega$ | rotation tensors |
| $S$ | strain tensors |


## ACKNOWLEDGMENTS

Financial support for this work was provided by the Aviation Engine and Gas Turbine Basic Science Center Project of China (P2022-B-II-008-001) and Technology Major Project of China (No: J2019-II-0009- 0029) greatly appreciated.


## REFERENCES


[1] Zhongqi, W, Renbian. Q. (1981). Principle of Turbomachinery. *Beijing: Mechanical Industry Press*, pp. 20-45.

[2] Zhengping, Z. Yu, L. and Mars, L. etc. (2007). Research progress of turbomachinery technology of civil high bypass ratio turbofan engine. *China Aviation Society. High-Level Forum on Key Technologies of Large Aircraft and Proceedings of 2007 Annual Meeting of China,* pp. 225-244.

[3] Jie, G. and Qun, Z. (2013). Effect of tip groove shape on aerodynamic performance of rotor blades. *Journal of Aeronautics*, 34 (2), pp. 218-226.

[4] Sieverding C H. (2004). Understanding secondary flows in turbine blading. In: Proceedings of the State-of-the-Art & Impact on Blade Design, Gas Turbine Engineering Lecture Series.

[5] Langston L S. (2001). Secondary flows in axial turbines—A review. *Ann N Y Acad Sci*, 934 (1), pp. 11-26.

[6] Yonggang, Z. (2009). *Experimental Study on Aerodynamic Characteristics of Turbine Cascade.* MA. North China Electric Power University (Beijing).

[7] Mayle, R, E. (1991). The role of laminar-turbulent transition in gas turbine engines. *ASME Journal of Turbomachinery*, 113(4), pp. 509-537.

[8] Hourmouziadis, J. (1989). Aerodynamic design of low-pressure turbines[C]//*AGARD Lecture Series.* pp. 167.

[9] Jian, Y. (2008) . Large-eddy simulation of blade boundary layer spatio-temporal evolution under unsteady disturbances. PhD. Beijing University of Aeronautics and Astronautics.

[10] Weiyang, Q. Lei, Z. and Hualing, L. et al. (2012). Measurement of the transition and separation for turbine blade boundary layer with low-Reynolds number. *Journal of Propulsion Technology*, 33(6), pp. 859-865.

[11] Long, Y. Yunfei, W. Yanping, S. and Fu., C. (2001). Effect of Reynolds number on aerodynamic performance of low-pressure turbine. *Chinese Journal of Electrical Engineering*, 42 (03), pp. 1043-1052.

[12] Fusheng, M. (2020). Research on flow and heat transfer characteristics and improvement schemes of large meridian expansion turbine. Ph.D. Harbin Engineering University.

[13] Curits, E, M. Hodson, H, P. Banieghbal, M, R. et al. (1997). Development of blade profiles for low-pressure turbine applications. *ASME Journal of Turbomachinery*, 119(3), pp. 531-538.

[14] Huiling, C. Xingshuang, W, Tianrong, T. Liqi, S. Fulin, L. (2002). Effects of wake on boundary layer flow on suction surface of low-pressure turbine. *Aeroengine*, 48 (05), pp. 65-72.

[15] Chang 'an, T. (2021). Study on the influence mechanism of wake shape on the flow of high-load low-pressure turbine. PhD. Dalian University of Technology.